




Ecofriendly synthesis, crystal chemistry, electrical, and low-temperature magnetic properties of nanoparticles (Li–Cr) for drug delivery and MRI applications

D. Ravinder^{1,*} , D. Ravinder Nayak¹, Sridhar Rapolu², Khalid Mujasam Batoo³, Emad H. Raslan⁴, and Mohammad Hadi⁴

¹Department of Physics, Osmania University, Hyderabad, Telangana 500007, India

²Department of Basic Science and Humanities, Vignan Institute of Technology and Science, Deshmukhi (V), Yadadri-Bhuvanagiri (Dist), Hyderabad 508 284, Telangana, India

³King Abdullah Institute for Nanotechnology, King Saud University, P.O. Box-2455, Riyadh 11451, Saudi Arabia

⁴Department of Physics, College of Science, King Saud University, P.O. Box-2455, Riyadh 11451, Saudi Arabia

Received: 4 September 2020

Accepted: 16 November 2020

Published online:

2 January 2021

© Springer Science+Business Media, LLC, part of Springer Nature 2021

ABSTRACT

Mixed $\text{Li}_{(0.5-x/2)}\text{Fe}_{(2.5-x/2)}\text{Cr}_x\text{O}_4$ ($X = 0.0, 0.2, 0.4, 0.6, 0.8, 1.0$) nano-ferrite system was synthesized by using Citrate gel auto-combustion method. Structural parameters such as lattice constant, hopping length, and X-ray density were reported and discussed with composition. The surface morphology was presented and explained with TEM analysis and SAED patterns. XRD patterns show the prepared samples are single-phase cubic spinel structure and the average particle size lies between 17 to 27 nm. TEM analysis shows prepared sample are the crystallite formation in nano-size. DC electrical properties presented variation with temperature and composition were discussed and studied well behind the Curie temperature. Magnetic measurements are carryout with VSM (Vibrating Sample Magnetometer), Observations have shown that magnetic properties are strongly influenced due to the substitution of Cr^{3+} in Lithium ferrites. Two samples $\text{Li}_{0.5}\text{Cr}_{0.6}\text{Fe}_{1.9}\text{O}_4$ and $\text{Li}_{0.5}\text{Cr}_{1.0}\text{Fe}_{1.5}\text{O}_4$ were subjected to an applied field of 100 Oe between 5 and 375 K temperature for ZFC and FC (Zero Field Cooled and Field Cooled) measurements of magnetization which indicated blocking temperature at around 350 K for both samples beyond which they exhibited super-paramagnetic behavior.

Address correspondence to E-mail: ravindergupta28@rediffmail.com

1 Introduction

In the field of science and technology, nano-scale materials play an very important role because the nanostructure magnetic materials show evidence of novel properties and all other properties together are different than that of their bulk materials [1–3]. Hence, nano-size materials are the most important because nano-size material structure, magnetic and electrical properties studies, and their interrelation is still incomplete. Among magnetic materials, spinel are the most significant materials for research in fundamental electronic components due to their tremendous magnetic and electrical properties [4, 5].

Ferrites exhibit low loss behavior and high resistivity which make them highly potential in applications related to memory devices, electrical components, and microwave devices over a large frequency range [6–12]. Lithium ferrite has inverse spinel structure with Li^+ ions occupying B sites and Fe^{3+} occupying A sites [13, 14]. Lithium ferrite has been a widely investigated material due to its importance in construction and engineering of many electromagnetic and microwave devices [15, 16]. As well as doped lithium ferrites are performance wise more advantageous over other spinel structures and hence used in microwave devices that include circulators, gyrators, isolators, cathode materials, phase shifters, and memory cores because of their high curie temperature, low eddy current loss, high resistivity, high saturation magnetization, and hysteresis loop properties [17–20].

Various synthesis routes such as sol–gel and citrate, flash combustion, co-precipitation, and technique of microwave hydrothermal high-temperature ceramic methods play an important role in synthesis and good physio-chemical properties of ferrites [21]. Out of these methods, citrate gel auto-combustion attracts more attention as it is associated with processing at low temperature, less time, equivalent distribution of reactants, ability of producing particles of nano-size. Several investigations carried on Lithium–Cadmium [22], Lithium–Zinc [23], and Lithium–Magnesium [24] properties have been reported. From a review of earlier work, it is evident that very less attention has been paid to the study of structural, electrical, and magnetic properties in systematic manner. This paper reports the electrical, structural characterization, and magnetic properties of Cr-doped $\text{Li}_{(0.5-x/2)}\text{Fe}_{(2.5-x/2)}\text{Cr}_x\text{O}_4$ ($X = 0.0, 0.2,$

0.4, 0.6, 0.8, 1.0) nano-ferrites synthesized through citrate gel method.

2 Experimental details

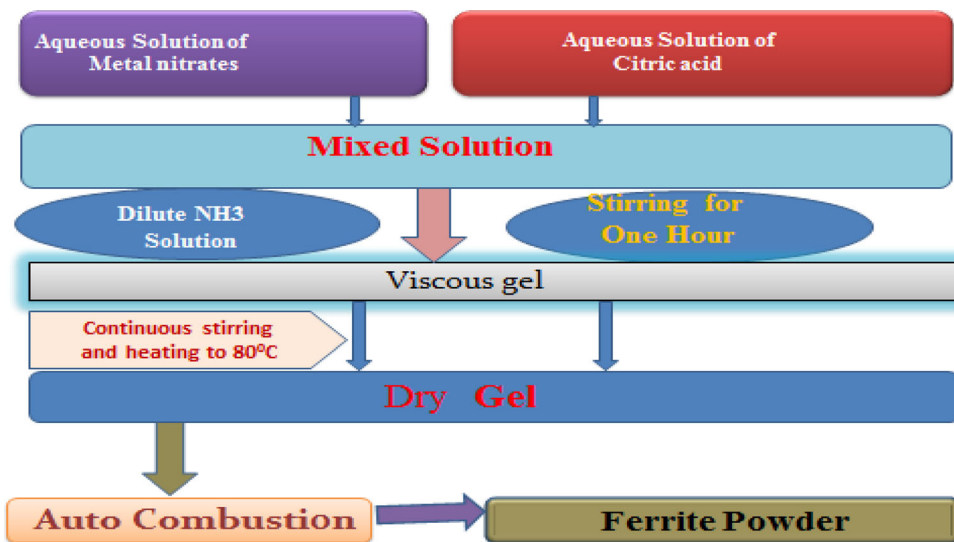
2.1 Materials

High-purity AR-grade Lithium Nitrate- $\text{Li}(\text{NO}_3)$, Chromium Nitrate- $(\text{Cr}(\text{NO}_3)_2 \cdot 9\text{H}_2\text{O})$, Citric Acid- $(\text{C}_6\text{H}_8\text{O}_7 \cdot \text{H}_2\text{O})$, Ferric Nitrate- $(\text{Fe}(\text{NO}_3)_3 \cdot 9\text{H}_2\text{O})$, and Ammonia(NH_3) are being used as starting materials to prepare Cr-doped $\text{Li}_{(0.5-x/2)}\text{Fe}_{(2.5-x/2)}\text{Cr}_x\text{O}_4$ ($X = 0.0, 0.2, 0.4, 0.6, 0.8, 1.0$) ferrite nanoparticles.

2.2 Synthesis of chromium-doped lithium ferrites

Synthesizing of nanoparticles from $\text{Li}_{(0.5-x/2)}\text{Fe}_{(2.5-x/2)}\text{Cr}_x\text{O}_4$ ($X = 0.0, 0.2, 0.4, 0.6, 0.8, 1.0$) ferrites was done by mixing the starting material in stoichiometric method with deionized water and nanoferrite samples were prepared by citrate gel auto-combustion method by taking the required molar ratio of citric acid and metal nitrates. The metal nitrates solutions are mixed together in beaker and the citric acid was added in 1:3 ration of nitrate to citric acid. Nitrate material work as oxidizing agent, whereas organic fuels act as reducing agents. By changing the oxidant to fuel sample ratio, properties of different materials were altered in sequential manner. The mixed solution was placed on magnetic stirrer with hot plate for 1 h maintaining temperature at 80 °C to get homogeneity. To this nitrate-citrate mixture, the ammonia is added slowly to maintain the pH to 7. The mixed solution was then heated at same temperature with uniform stirring to acquire a viscous gel which was further heated by a hot plate with temperature ranging between 180 to 200 °C. Removal of water molecules from the mixture takes place and foams the viscous gel resulting in formation of dry gel which produces ferrite powder particles on subjected to auto-combustion process. Finally, the ferrite powder particles were grained with Agate Mortar and Pestle and calcined (oxidized) in a muffle furnace at a temperature of 700 °C for 5 h which was once again grained to obtain better crystallization and homogeneity in the spinel. Figure 1 represents the flow chart of synthesis of present materials.

Fig. 1 Flow chart for the preparation of $\text{Li}_{(0.5-x)/2}\text{Fe}_{(2.5-x/2)}\text{Cr}_x\text{O}_4$ ($X = 0.0, 0.2, 0.4, 0.6, 0.8, 1.0$) nanoparticles



The structural characterization was carried out by X-ray Diffractometer (Model 3710-Philips) using $\text{CuK}\alpha$ radiation ($\lambda = 1.5405 \text{ \AA}$) at normal temperature through continuous scanning between 10° to 80° (Bragg's angles) in steps of $0.04^\circ/\text{s}$.

The average crystallite size of nano-ferrites was calculated from the most intense peak (311) according to Debye Scherer's formula [25]:

$$D = 0.91\lambda / \beta \cos\theta$$

where the X-ray wavelength is given by ' λ ' and FWHM in radians is ' β '.

The lattice parameter has been determined from the relation:

$$a = d * \sqrt{h^2 + k^2 + l^2}$$

The density of X-ray ' d_x ' was found using the relation [26]:

$$d_x = \frac{nM}{a^3N} \text{ g/cm}^3$$

where ' M ' and ' N ' correspond to samples molecular weight and Avogadro number.

The hopping length at A and B sites were calculated from the formula [27]:

$$L_A = \frac{a\sqrt{3}}{4} \quad L_B = \frac{a\sqrt{2}}{4}$$

The doping effect always results into the strain in the base matrix. The effect of Cr^{3+} doping on the local strain was calculated according to the formula:

$$\varepsilon = \frac{\beta \cos\theta}{4}$$

The stress was calculated according to the formula:

$$\delta = \frac{15 - \varepsilon}{a \cdot t}$$

Morphology of the samples and average particle size were measured and discussed through TEM (Tecnai-12, FEI, Netherlands) and SAED analysis (Transmission Electron Microscopy and Selected Area Electron Diffraction).

DC electrical properties as a function of temperature between 200 to 600 °C and composition were calculated with the help of two-probe method [17].

The resistivity (ρ) and temperature (T) Kelvin relationship may be expressed as Arrhenius relation [28]:

$$\rho = \rho_0 e^{\Delta E / K_B T}$$

which ρ_0 denote the resistivity at normal room temperature, ' K_B ' represents Boltzmann constant, and ' ΔE ' stands for activation energy.

Activation energy can be determined using the following equation:

$$\Delta E = 2.303 \times K_B \times 10^3 \times \text{slope (eV)}$$

Vibrating sample magnetometer (GMW Magnet System, model 3473) was performed at 310 K and 5 K (high and low) temperatures in order to measure Remanence Magnetization (M_r) and Coercivity (H_c). Magnetization measurements ZFC-FC for two particular ferrite compositions $\text{Li}_{0.5}\text{Cr}_{0.6}\text{Fe}_{1.9}\text{O}_4$ and

$\text{Li}_{0.5}\text{Cr}_x\text{Fe}_{1.5}\text{O}_4$ were carried out in the range of 5–360 K temperature on application of magnetic field (H) equal to 100 Oe.

3 Results and discussion

3.1 XRD

Figure 2 shows the XRD pattern of Li–Cr nano-ferrite system which demonstrates XRD and crystalline phases that are noticed and evaluated with reference data of PDF-4 from ICDD (International Centre for Diffraction Data). The XRD indicated strong reflection from (311) plane confirming spinel phase structure, while other reflections from (220), (222), (400), (422), (511), and (440) planes confirm cubic unit cell. Therefore, single-phase cubic spinel structure of Fd_3m space group without displaying other phases of impurity can be confirmed from these allowed planes.

Table 1 tabulates the calculated values of structural parameters D , a , d_x (crystallite size, lattice parameter, X-ray density), and hopping length at A, B sites from which it is observed that the average crystallite size is in nanometer range between 27 to 17 nm. Increase in concentration of chromium decreases lattice parameter in Li ferrites because the ionic radii of the Cr^{3+} (62 Å) are smaller than the ionic radii of the Fe^{3+} (69 Å). X-ray density decreases with increasing chromium concentration in Li ferrites due to decrease in lattice parameter. These reports are in good

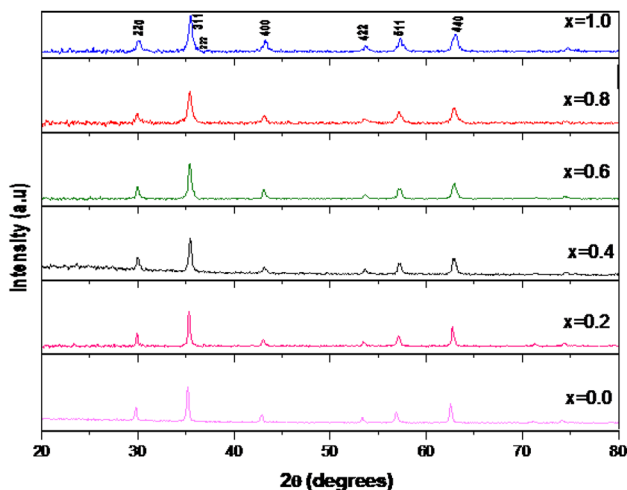


Fig. 2 XRD pattern of the $\text{Li}_{(0.5-x/2)}\text{Fe}_{(2.5-x/2)}\text{Cr}_x\text{O}_4$ ($X = 0.0, 0.2, 0.4, 0.6, 0.8, 1.0$) nano-ferrites

agreement with others (Latta and Ravinder [29] in case of Mn–Zn ferrites, West and Blankenship [30] in case of Li–Zn ferrites). The values of hopping length are found to increase at A, B sites with increase in Cr^{3+} content (x) in Li ferrites. The observed stress and strain values increase with increase in Cr^{3+} doping in Li ferrites, because of decreasing the size of the particles and also due to the incorporation a smaller Cr^{3+} ion at larger Fe^{3+} ion.

3.2 Morphological study

One of the important characteristics of nano-scale material is shape and its particle size distribution. Figure 3 represents the TEM micrographs of synthesized Li–Cr nano-ferrite system which shows that the particles are accumulated one on another because of mutual magnetic attraction between them and the prepared samples exhibit comparatively uniform particle distribution around 20 nm having the shape of a polyhedral. TEM images show agglomerated nanoparticles with collection of different nanograins isolated from each other and spherical in shape [19, 31].

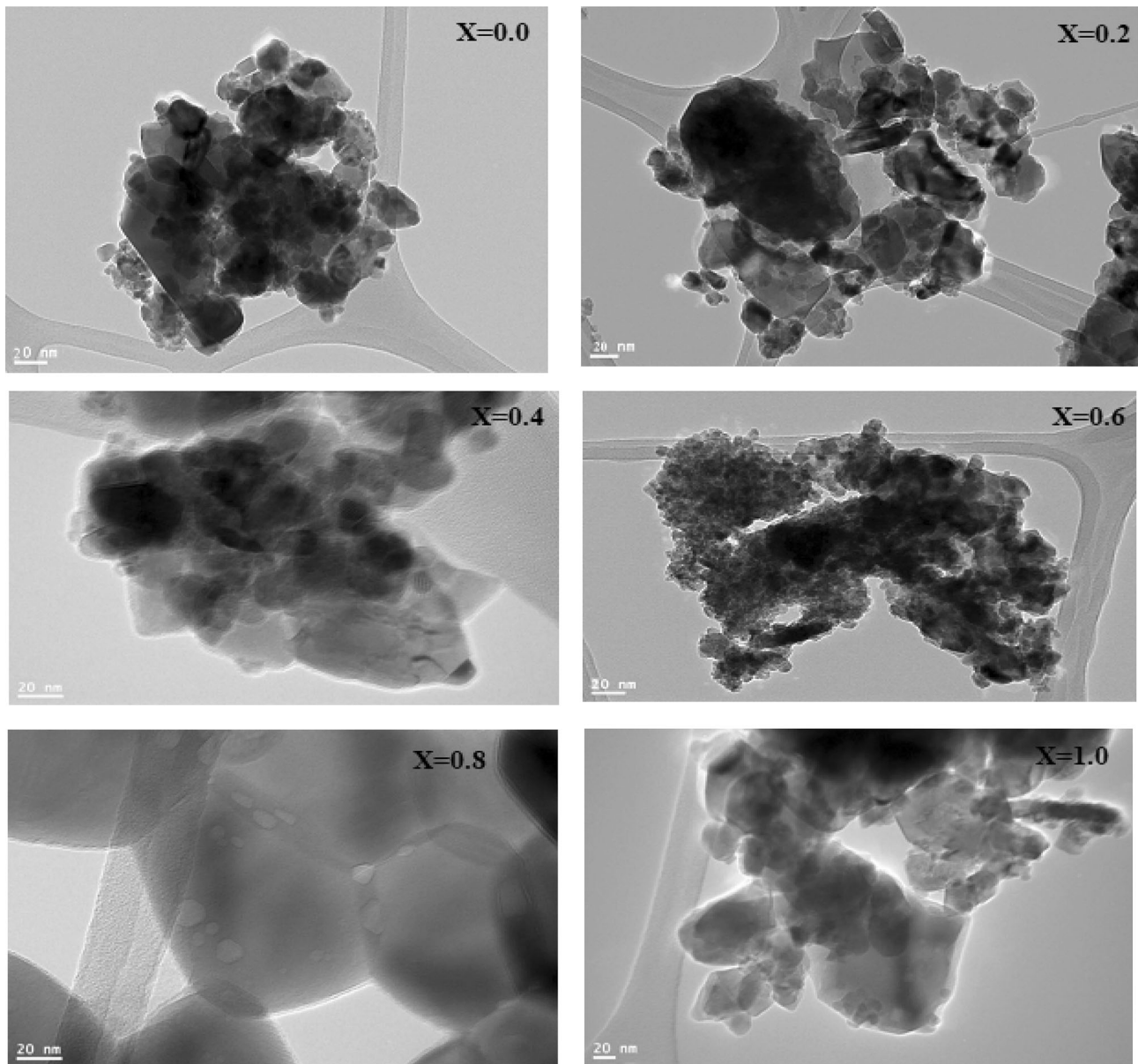
Figure 4 represents the SAED patterns of the prepared sample for $x = 0.00$ and $x = 0.80$ which illustrates that ferrite nanoparticles doped with Cr^{3+} originate with well-crystalline nature. The superimposition between bright spot and Debye ring pattern clearly identifies the nature to be polycrystalline and the patterns clearly approve the particles to be crystallite and nano-sized.

3.3 DC electrical properties

DC electrical measurement is an influential technique to illuminate the electrical conductivity mechanism. Hopping mechanism accounts for electrical conduction in ferrites [32]. Variation in DC conductivity with temperature between 200 and 600 °C for $\text{Li}_{(0.5-x/2)}\text{Fe}_{(2.5-x/2)}\text{Cr}_x\text{O}_4$ ($X = 0.0, 0.2, 0.4, 0.6, 0.8, 1.0$) nano-ferrites is reported. Figure 5a–f demonstrate the graphs for $\ln(\sigma T)$ versus $1000/T$ from which it can be seen that increase in temperature increases conductivity (σ) for each sample prepared exhibiting normal semiconductor behavior [33]. From the plots of Arrhenius, graph of $\ln(\sigma T)$ versus $10^3/T$ divided the curve into two regions (known as curie temperature) resulting in ferrimagnetic region and paramagnetic region which is known to be the change of magnetic

Table 1 The Structural characterization parameters of $\text{Li}_{(0.5-x/2)}\text{Fe}_{(2.5-x/2)}\text{Cr}_x\text{O}_4$ ($X = 0.0, 0.2, 0.4, 0.6, 0.8, 1.0$) nano-ferrites

Cr^{3+} content (x)	Crystallite size (nm) ± 0.2 nm	Lattice parameter (Å)	X-ray density (d_x)	Stain (ϵ)	Stress (δ)	Hoping length	
						A-site (d_A) Å	B-site (d_B) Å
$X = 0.0$	27	8.433	4.760	0.050	0.065	3.6080	2.9458
$X = 0.2$	21	8.414	4.600	0.046	0.0846	3.6433	2.9744
$X = 0.4$	26	8.401	4.611	0.070	0.0683	3.6328	2.9661
$X = 0.6$	21	8.400	4.587	0.090	0.0845	3.6375	2.9697
$X = 0.8$	21	8.397	4.575	0.085	0.0847	3.6361	2.9685
$X = 1.0$	17	8.381	4.565	0.085	0.1046	3.6289	2.9626

**Fig. 3** TEM Images of $\text{Li}_{(0.5-x/2)}\text{Fe}_{(2.5-x/2)}\text{Cr}_x\text{O}_4$ ($X = 0.0, 0.2, 0.4, 0.6, 0.8, 1.0$) ferrite nanoparticle

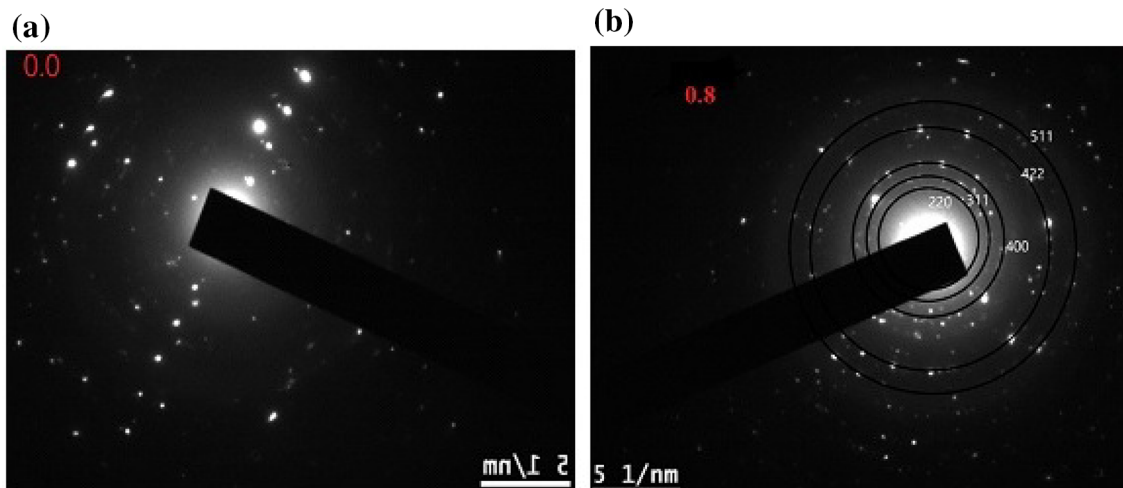


Fig. 4 SAED pattern for the composition **a** $\text{Li}_{0.5}\text{Fe}_{2.5}\text{O}_4$ and **b** $\text{Li}_{0.1}\text{Cr}_{0.8}\text{Fe}_{2.1}\text{O}_4$

ordering. Hence two activation energies in low- and high-temperature regions which are at below Curie and above Curie temperature are achieved due to change in magnetic state.

Table 2 lists the values obtained for activation energy and curie temperature in ferrimagnetic and paramagnetic regions. It was observed that increase in concentration of Cr^{3+} decreases Curie temperature in lithium ferrite, which may be attributed to reduction in magnetic exchange interaction between the B and A sites [34]. According to magnetic semiconductor theory, regions of ferromagnetic are ordered, while regions of paramagnetic are disordered [35]. Hence conduction in the paramagnetic region requires more energy as compared to ferrimagnetic region. Hence, activation energy in paramagnetic region (E_p) is more than the other (E_f) [36–38] which can be achieved with small value of electrical conductivity in paramagnetic region, whereas it requires high value of electrical conductivity for same energy in ferrimagnetic region.

3.4 Magnetic properties

Measurements of variation in magnetization with temperature was studied with VSM (Vibrating Sample Magnetometer) for $\text{Li}_{0.5}\text{Cr}_{0.6}\text{Fe}_{1.9}\text{O}_4$ and $\text{Li}_{0.5}\text{Cr}_{1.0}\text{Fe}_{1.5}\text{O}_4$ samples at 5 K and 310 K temperatures on application of ± 10 T magnetic field. The ZFC (Zero field cooled) measurements were observed during cooling without any magnetic field FC (Field cooled) measurements were observed by heating with applied magnetic field of 100 Oe.

Figure 6a and b illustrate ZFC (Zero Field Cooled) and FC (Field Cooled) conditions for $\text{Li}_{0.5}\text{Cr}_{0.6}\text{Fe}_{1.9}\text{O}_4$ and $\text{Li}_{0.5}\text{Cr}_{1.0}\text{Fe}_{1.5}\text{O}_4$ samples on applying 100 Oe magnetic field. It demonstrated that decrease in temperature increases FC magnetization curve, while the curve related to ZFC magnetization is super maximum for specific temperature. The divergence observed between FC and ZFC curves is about 350 K which is called blocking temperature (T_b). This is due to super-paramagnetic behavior present in the sample. Beyond blocking temperature, magnetic moment of single domain nanoparticle might be unblocked continuously. Finally, the $M-H$ curve reaches a position of thermal equilibrium similar to an atomic paramagnet [39].

Figure 7a and b illustrate magnetic hysteresis loops for samples $\text{Li}_{0.5}\text{Cr}_{0.6}\text{Fe}_{1.9}\text{O}_4$ and $\text{Li}_{0.5}\text{Cr}_{1.0}\text{Fe}_{1.5}\text{O}_4$ on application of ± 10 T magnetic field at 5 K and 310 K temperatures which indicated clearly that the two samples exhibit ferrimagnetic behavior. These hysteresis loops were used to measure coercivity (H_c) and remanence magnetization (M_r) whose values are reported in Table 3. Observations show that increase in temperature decreases the magnetic behavior of samples under investigation. Reports indicate similar results with varying compositions synthesized by various methods [40, 41].

Comparison between FC–ZFC and hysteresis data clearly indicated that the material show some hysteresis behavior as ferrimagnetic material below blocking temperature and above this temperature the material behaves to be super-paramagnetic with disappearance of hysteresis. Hence, Lithium–

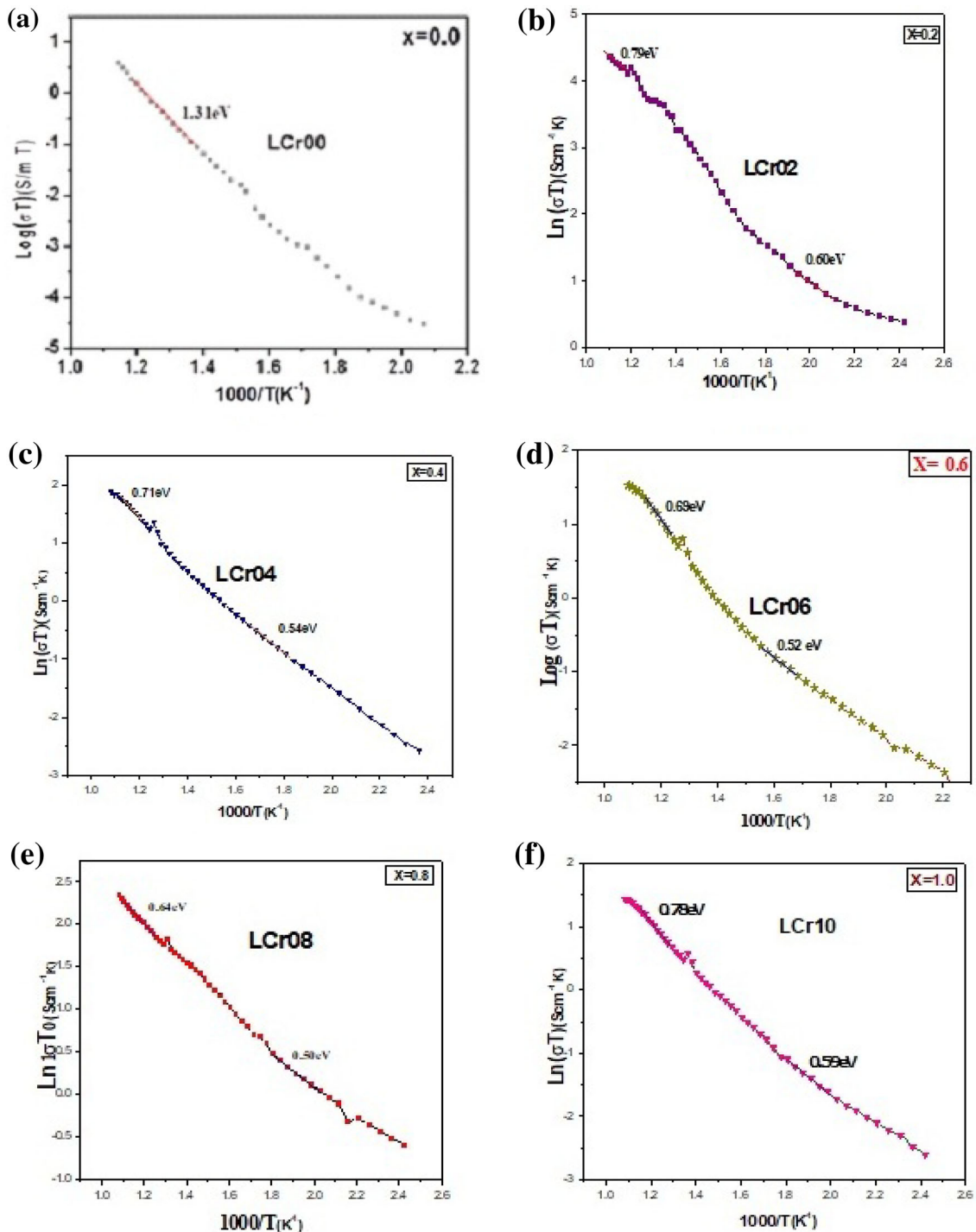


Fig. 5 a–f DC Conductivity variation with temperature of $\text{Li}_{(0.5-x/2)}\text{Fe}_{(2.5-x/2)}\text{Cr}_x\text{O}_4$ ($X = 0.0, 0.2, 0.4, 0.6, 0.8, 1.0$) nano-ferrite system

Chromium nano-ferrites amid super-paramagnetic behavior makes them highly potential for transformers cores, inductor devices, recording heads, and in bio-medical applications specific to drug delivery and MRI (Magnetic Resonance Imaging).

4 Conclusion

Synthesized Li–Cr nano-ferrite samples with Citrate gel auto-combustion technique shows cubic spinel structure with average particle size between 17 and 27 nm. X-ray density and lattice constant decrease

Table 2 Electrical resistivity and activation energies of $\text{Li}_{(0.5-x/2)}\text{Fe}_{(2.5-x/2)}\text{Cr}_x\text{O}_4$ ($X = 0.0, 0.2, 0.4, 0.6, 0.8, 1.0$) nano-ferrite system

Composition	Curie temperature (K)	Activation energy (eV)	
		Ferrimagnetic region	Paramagnetic region
$\text{Li}_{0.5}\text{Fe}_{2.5}\text{O}_4$	600	1.34	–
$\text{Li}_{0.4}\text{Cr}_{0.2}\text{Fe}_{2.4}\text{O}_4$	572	0.875	0.945
$\text{Li}_{0.3}\text{Cr}_{0.4}\text{Fe}_{2.3}\text{O}_4$	560	0.703	0.798
$\text{Li}_{0.2}\text{Cr}_{0.6}\text{Fe}_{2.2}\text{O}_4$	553	0.526	0.659
$\text{Li}_{0.1}\text{Cr}_{0.8}\text{Fe}_{2.1}\text{O}_4$	540	0.480	0.621
CrFe_2O_4	520	0.575	0.712

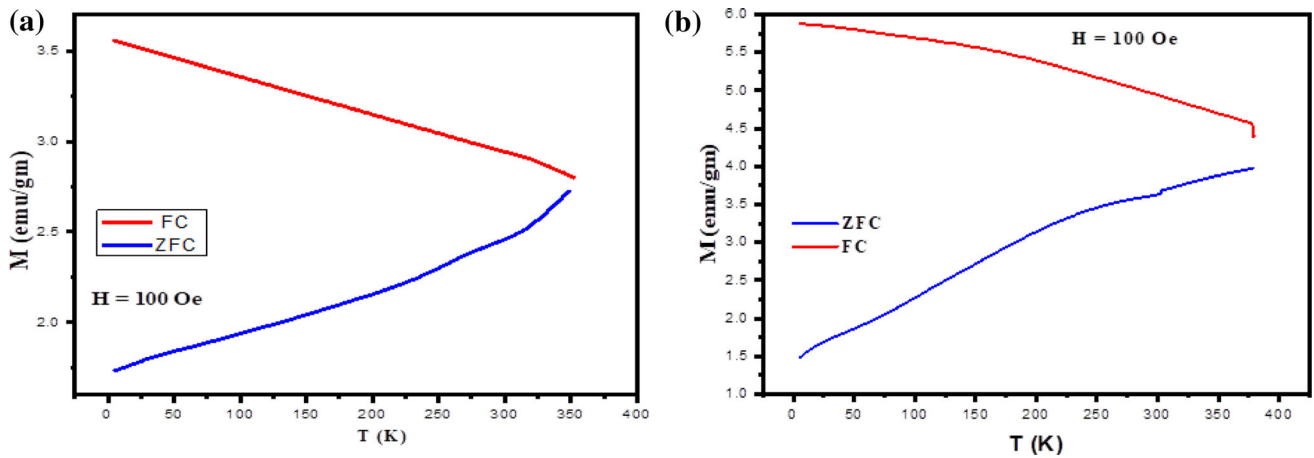


Fig. 6 a, b ZFC and FC for $\text{Li}_{0.5}\text{Cr}_{0.6}\text{Fe}_{1.9}\text{O}_4$ and $\text{Li}_{0.5}\text{Cr}_{1.0}\text{Fe}_{1.5}\text{O}_4$

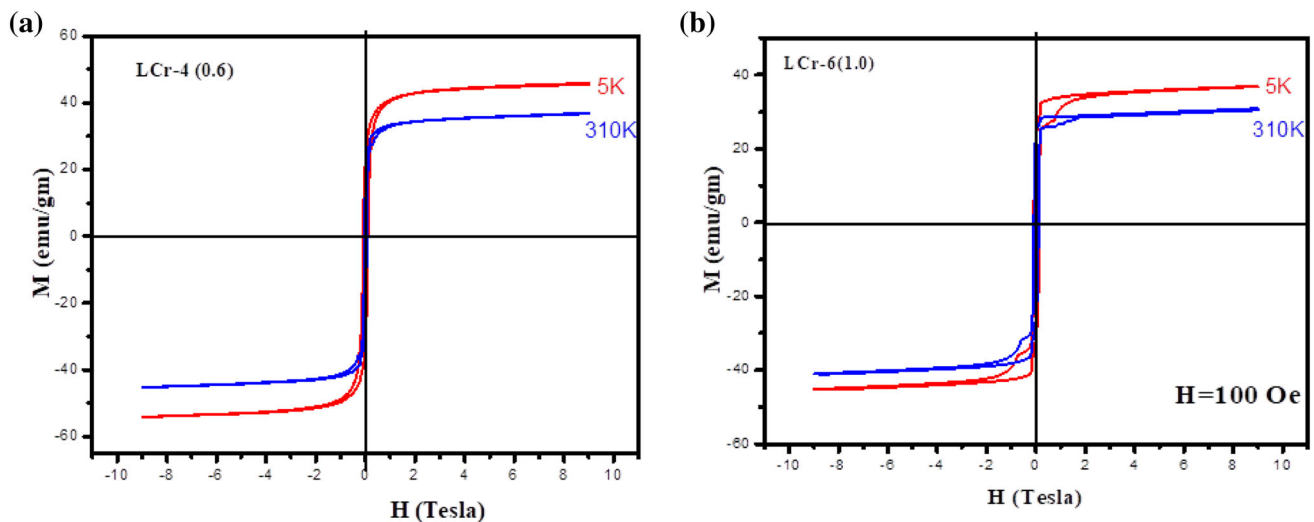


Fig. 7 a, b Hysteresis Curves for $\text{Li}_{0.5}\text{Cr}_{0.6}\text{Fe}_{1.9}\text{O}_4$ and for $\text{Li}_{0.5}\text{Cr}_{1.0}\text{Fe}_{1.5}\text{O}_4$ at 5 K and 310 K

with increased chromium concentration in Li ferrites. TEM images show that most of the nanoparticles are agglomerated with collection of various nanograins isolated from each other that are spherical in shape. The SAED patterns show that the particles are crystallite and nano-sized. DC conductivity variation

with temperature explains that the prepared samples show the normal behavior of semiconductor nature. As a result of the FC–ZFC and hysteresis information, Li–Cr nano-ferrites amid super-paramagnetic behavior are attractive for transformers cores, inductor devices, recording heads, and in bio-medical

Table 3 Magnetic parameters of $\text{Li}_{0.5}\text{Cr}_{0.6}\text{Fe}_{1.9}\text{O}_4$ and $\text{Li}_{0.5}\text{Cr}_{1.0}\text{Fe}_{1.5}\text{O}_4$

Magnetic parameters	$\text{Li}_{0.5}\text{Cr}_{0.6}\text{Fe}_{1.9}\text{O}_4$		$\text{Li}_{0.5}\text{Cr}_{1.0}\text{Fe}_{1.5}\text{O}_4$	
	310 K	5 K	310 K	5 K
Coercivity (H_c)	0.037	0.082	0.085	0.097
Remanence (M_r) (emu/g)	14.43	23.44	21.18	22.47

applications specific to drug delivery and MRI (Magnetic Resonance Imaging).

Acknowledgements

The authors are very grateful to Prof. G. Prasad, Head, Department of Physics, University College of Science, Osmania University, Hyderabad. One of the authors D.R is grateful to Osmania University, UPE-FAR and Osmania University, DST PURSE New Delhi for their financial assistance. KM Batoo is thankful to the Deanship of Scientific Research at King Saud University for financial support through the project code (Grant No. RG-1437-030).

References

- Z. Gao, B. Xu, M. Ma, A. Feng, Y. Zhang, X. Liu, Z. Jia, G. Wu, *Compos. B* **179**, 107417 (2019)
- S.B. Somvanshi, S.R. Patade, D.D. Andhare, S.A. Jadhav, M.V. Khedkar, P.B. Kharat, P.P. Khirade, K.M. Jadhav, *J. Alloys Compd.* **835**, 155422 (2020)
- Z. Lou, R. Li, P. Wang, Y. Zhang, B. Chen, C. Huang, C. Wang, H. Han, Y. Li, *Chem. Eng. J.* **391**, 123571 (2020)
- R.M. Borade, S.B. Somvanshi, S.B. Kale, R.P. Pawar, K. Jadhav, *Mater. Res. Express* **7**, 016116 (2020)
- P.B. Kharat, S. More, S.B. Somvanshi, K. Jadhav, *J. Mater. Sci.* **30**, 6564–6574 (2019)
- A. Abou-Hassan, S. Neveu, V. Dupuis, V. Cabuil, *RSC Adv.* **2**, 11263–11266 (2012)
- M. Babrekar, K. Jadhav, *Int. Res. J. Sci. Eng.* **1**, 73–76 (2017)
- R. Supriya, D. Andhare Deepali, B. Somvanshi Sandeep, B. Kharat Prashant, D. Santosh, M. Jadhav Kamalakar, *Nanomater. Energy* **9**, 8–13 (2020)
- H.J. Kardile, S.B. Somvanshi, A.R. Chavan, A.A. Pandit, K.M. Jadhav, *Optik* **207**, 164462 (2020)
- Q. Yue, C. Liu, Y. Wan, X. Wu, X. Zhang, P. Du, *J. Catal.* **358**, 1–7 (2018)
- S. Caspani, R. Magalhães, J.P. Araújo, *Materials* **13**, 2586 (2020)
- B. Chen, Z. Guo, C. Guo, Y. Mao, Z. Qin, D. Ye, F. Zang, Z. Lou, Z. Zhang, M. Li, Y. Liu, *Nanoscale* **12**, 5521–5532 (2020)
- S. Verma, P.A. Joy, *J. Appl. Phys.* **98**, 124312 (2005)
- D.E. Zhang, W. Shu, S. Li, X. Zhang, A. Ying, Z. Tong, *J. Mater. Sci.* **43**, 5948–5951 (2008)
- A.V. Humbe, P.B. Kharat, A.C. Nawle et al., *J. Mater. Sci.* **29**, 3467–3481 (2018)
- P.B. Kharat, J.S. Kounsalye, M.V. Shisode et al., *J. Supercond. Nov. Magn.* **32**, 341–351 (2019)
- P.B. Kharat, M.V. Shisode, S.D. Birajdar, D.N. Bhojar, K.M. Jadhav, *AIP Conf. Proc.* **1832**, 050122 (2017)
- P.B. Kharat, S.B. Somvanshi, P.P.K.K.M. Jadhav, *J. Phys.* **1644**, 12028 (2020)
- Y.P. Fu, C.S. Hsu, *Sol. Stat. Comm.* **134**, 201 (2005)
- D. Ravinder, L. Balachander, Y.C. Venudhar, *Mater. Lett.* **49**, 267 (2001)
- S.B. Somvanshi, S.A. Jadhav, M.V. Khedkar, P.B. Kharat, S.D. More, K.M. Jadhav, *Ceram. Int.* **46**(9), 13170 (2020)
- S.S. Bellad, R.B. Pujar, B.K. Chougule, *Mater. Chem. Phys.* **52**, 166 (1998)
- D. Ravinder, *J. Mater. Sci. Lett.* **11**, 1498 (1992)
- Y. Purushotham, M.B. Reddy, P. Kishan, D.R. Sagar, P. Raghasudha, M. Ravinder, D. Veerasomaiah, *Adv. Mater. Lett.* **4**, 910 (2013)
- K. Latta, D. Ravinder, *Phys. Stat. Soli. A* **139**, 109 (1993)
- K.M. Batoo, E.H. Raslan, Y. Yang, S.F. Adil, M. Khan, A. Imran, Y. Al-Douri, *AIP Adv.* **9**, 055202 (2019)
- M.C. Varma, G.S.V.R.K. Choudary, A.M. Kumar, K.H. Rao, *Phys. Res. Inter.* **1**, 579745 (2014)
- P.P. Hankare, R.P. Patil, U.B. Sankpal, S.D. Jadhav, I.S. Mulla, K.M. Jadhav, B.K. Chougule, *J. Magn. Magn. Mater.* **321**, 3270 (2009)
- A.A. Sattar, H.M. El-Shokrofy, M.M. El-Tabey, *J. Appl. Sci.* **5**, 162–168 (2005)
- R.G. West, A.C. Blankenship, *J. Am. Ceram. Soc.* **50**, 343 (1967)
- S. Jauhar, A. Goyal, N. Lakshmi, K. Chandra, S. Singhal, *Mater. Chem. Phys.* **139**, 836 (2013)
- Ferrite Material Science and Technology, *Narosa publishing house*, New Delhi (1990)
- V.D. Reddy, M.A. Malik, P.V. Reddy, *Mater. Sci. Eng. B* **8**(4), 295–301 (1991)
- K.C.B. Naidu, G. Suresh Kumar, N. Ranjith Kumar, *J. Aust. Ceram. Soc.* **1**, 1 (2018)
- D. Ravinder, K. Vijaya Kumar, B.S. Boyanor, *Mater. Lett.* **38**, 22–27 (1999)

36. K.C.B. Naidu, V.N. Reddy, T.S. Sarmash, D. Kothandan, T. Subbarao, N.S. Kumar, *J. Aust. Ceram. Soc.* **55**, 201–218 (2019)
37. D.S. Kumar, K.C.B. Naidu, M.M. Raf, K.P. Nazeer, A.A. Begam, G.R. Kumar, *Mater. Sci. Pol.* **36**, 123–133 (2018)
38. D. Sivakumar, K.C.B. Naidu, K.P. Nazeer, M.M. Raf, G. Rameshkumar, B. Sathyaseelan, G. Killivalavan, A.A. Begam, *J. Korean Ceram. Soc.* **55**, 230–238 (2018)
39. K.C.B. Naidu, W. Madhuri, *Bull. Mater. Sci.* **40**, 417 (2017)
40. S. Chander, M.P. Sharma, A. Krishnamurthy, B.K. Srivastava, *Ind. J. Pure Appl. Phys.* **45**, 816–820 (2007)
41. J. Henriques, E. Tatarova, F.M. Dias, C.M. Ferreira, *J. Appl. Phys.* **9**, 5632–5639 (2002)

Publisher's Note Springer Nature remains neutral with regard to jurisdictional claims in published maps and institutional affiliations.

Terms and Conditions

Springer Nature journal content, brought to you courtesy of Springer Nature Customer Service Center GmbH (“Springer Nature”).

Springer Nature supports a reasonable amount of sharing of research papers by authors, subscribers and authorised users (“Users”), for small-scale personal, non-commercial use provided that all copyright, trade and service marks and other proprietary notices are maintained. By accessing, sharing, receiving or otherwise using the Springer Nature journal content you agree to these terms of use (“Terms”). For these purposes, Springer Nature considers academic use (by researchers and students) to be non-commercial.

These Terms are supplementary and will apply in addition to any applicable website terms and conditions, a relevant site licence or a personal subscription. These Terms will prevail over any conflict or ambiguity with regards to the relevant terms, a site licence or a personal subscription (to the extent of the conflict or ambiguity only). For Creative Commons-licensed articles, the terms of the Creative Commons license used will apply.

We collect and use personal data to provide access to the Springer Nature journal content. We may also use these personal data internally within ResearchGate and Springer Nature and as agreed share it, in an anonymised way, for purposes of tracking, analysis and reporting. We will not otherwise disclose your personal data outside the ResearchGate or the Springer Nature group of companies unless we have your permission as detailed in the Privacy Policy.

While Users may use the Springer Nature journal content for small scale, personal non-commercial use, it is important to note that Users may not:

1. use such content for the purpose of providing other users with access on a regular or large scale basis or as a means to circumvent access control;
2. use such content where to do so would be considered a criminal or statutory offence in any jurisdiction, or gives rise to civil liability, or is otherwise unlawful;
3. falsely or misleadingly imply or suggest endorsement, approval, sponsorship, or association unless explicitly agreed to by Springer Nature in writing;
4. use bots or other automated methods to access the content or redirect messages
5. override any security feature or exclusionary protocol; or
6. share the content in order to create substitute for Springer Nature products or services or a systematic database of Springer Nature journal content.

In line with the restriction against commercial use, Springer Nature does not permit the creation of a product or service that creates revenue, royalties, rent or income from our content or its inclusion as part of a paid for service or for other commercial gain. Springer Nature journal content cannot be used for inter-library loans and librarians may not upload Springer Nature journal content on a large scale into their, or any other, institutional repository.

These terms of use are reviewed regularly and may be amended at any time. Springer Nature is not obligated to publish any information or content on this website and may remove it or features or functionality at our sole discretion, at any time with or without notice. Springer Nature may revoke this licence to you at any time and remove access to any copies of the Springer Nature journal content which have been saved.

To the fullest extent permitted by law, Springer Nature makes no warranties, representations or guarantees to Users, either express or implied with respect to the Springer nature journal content and all parties disclaim and waive any implied warranties or warranties imposed by law, including merchantability or fitness for any particular purpose.

Please note that these rights do not automatically extend to content, data or other material published by Springer Nature that may be licensed from third parties.

If you would like to use or distribute our Springer Nature journal content to a wider audience or on a regular basis or in any other manner not expressly permitted by these Terms, please contact Springer Nature at

onlineservice@springernature.com